International Journal of Solids and Structures 46 (2009) 617–634

Contents lists available at ScienceDirect

International Journal of Solids and Structures

journal homepage: www.elsevier.com/locate/ijsolstr

On the crushing of aluminum open-cell foams: Part I. Experiments

Wen-Yea Jang, Stelios Kyriakides *

Research Center for Mechanics of Solids, Structures & Materials, The University of Texas at Austin, WRW 110, C0600, Austin, TX 78712, USA

ARTICLE INFO

Article history:
Received 28 May 2008
Received in revised form 1 September 2008
Available online 19 September 2008

Keywords:
Foams
Aluminium
Crushing

ABSTRACT

This two-part study is concerned with the understanding and modeling of the compressive response of open-cell metallic foams. Part I presents experimental results from Al-6101-T6 foams of three different cell sizes with relative densities of about 8%. X-ray tomography is first used to characterize the geometry of the microstructure. The cells are irregular polyhedra of nearly uniform size that are somewhat elongated in one direction. The ligaments are nearly straight with convex, three-sided cross-sections and variable area distribution along their length. Foam specimens were compressed at slow displacement rates along the rise and transverse directions and the evolution of crushing in the specimens was monitored using X-ray tomography. In both directions, the response is initially nearly linear, terminating into a limit load that is followed by an extensive load plateau. At an average strain of about 55% the load increases monotonically again due to densification. The limit load is caused by plastification due to combined compression and bending of the ligaments. Beyond this point, cells start to buckle and collapse locally, forming bands that cover the full cross-section of the specimen. Contact of the collapsing cells arrests local deformation triggering collapse in neighboring cells. In this manner, crushing gradually spreads throughout the specimen and when this is achieved the load required for further deformation starts to rise. The initial elastic modulus, the stresses at the limit load and the plateau and the extent of the plateau have been measured as a function of relative density for both directions. The stress–displacement response in the transverse direction is generally somewhat lower than in the rise direction but the prevalent events were found to be similar in the two directions.

1. Introduction

Synthetic cellular materials can be manufactured with relative ease from all major material categories including metals, polymers, ceramics, and carbon using a foaming or another process (see Ashby et al., 2000). Of interest here are open-cell foams with relative densities of a few percent (~2–10% but can be as low as 0.3%) that consist of irregular polyhedra cells with anywhere from 9 to 17 faces (for nearly monodisperse foams, see Fig. 1). The material is concentrated in the nearly straight edges of the polyhedra and in the nodes where they intersect, usually four at a time. This microstructure is responsible for their unique properties (mechanical, thermal, acoustical, etc.) that are nicely summarized in Gibson and Ashby's book (1997) (see also Hilyard and Cunningham, 1994, Weaire and Hutzler, 1999, MRS Bulletin – Gibson, 2003). The design and use of such foams requires that the microstructure and the properties of the base material be related to the foam properties of interest. This work is concerned with the mechanical properties of metallic open-cell foams.

Fig. 2 shows the compressive stress– (σ_{11} = force/undeformed area) displacement (δ_1/H_1) response of an aluminum alloy open-cell foam that is characteristic of most foams open- as well as closed-cell (see also Zhou et al., 2002, 2004) It consists of

* Corresponding author.
E-mail address: skk@mail.utexas.edu (S. Kyriakides).

0020-7683/$ - see front matter © 2008 Elsevier Ltd. All rights reserved.
doi:10.1016/j.ijsolstr.2008.09.008

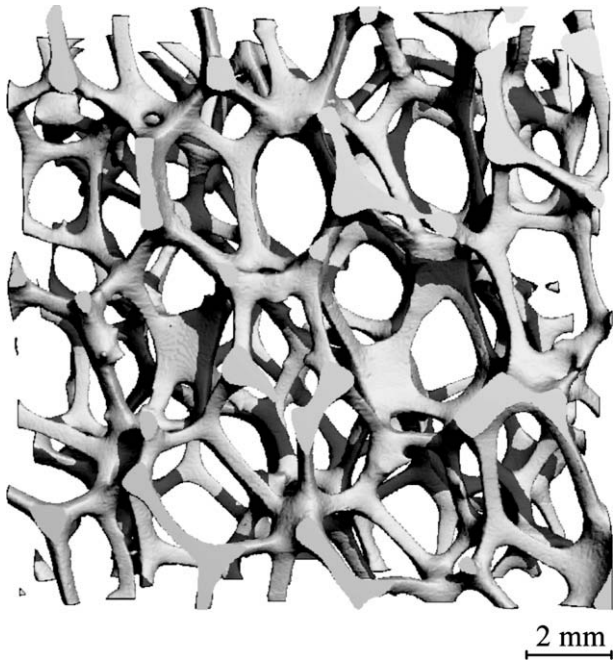

Fig. 1. Computed tomography image of a 10 ppi Al foam (ρ^*/ρ = 8.23%).

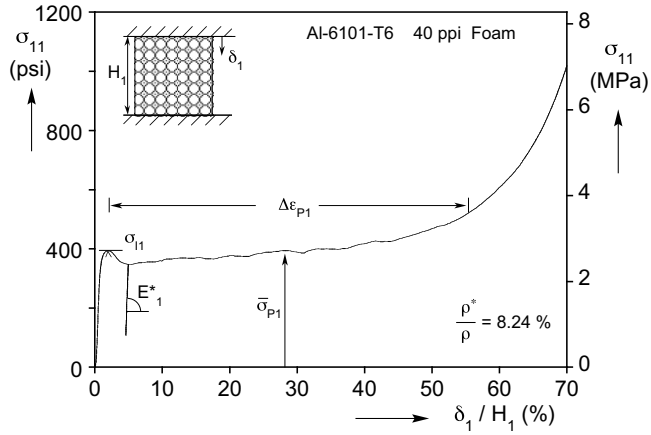

Fig. 2. Typical compressive response of an Al alloy open-cell foam (crushing in the rise direction Spec. R40-3).

a nearly linear elastic regime that terminates into a limit load (σ_l). This is followed by a load plateau that extends to an average strain of about 55% followed by a second stiff branch. The low initial stress peak and extended load plateau are responsible for the excellent energy absorption characteristics of such foams. The objective of this work is to relate the deformation history of the aluminum foam microstructure to the main variables of this response $\{E^*, \sigma_l, \bar{\sigma}_P, \Delta\varepsilon_P\}$.

Gong et al. (2005) and Gong and Kyriakides (2005) in a similar study on elastic polymeric open-cell foams demonstrated that their compressive response exhibited very similar characteristics to those in Fig. 2, albeit at much lower stress levels. They showed that the load peak corresponded to the onset of an instability affecting the whole domain tested, followed by localized crushing of cells in bands. During the stress plateau the bands multiplied and broadened. Once most of the cells were crushed, the response picked up again. These characteristics were reproduced numerically by idealizing the microstructure as regular Kelvin cells made to match the cell anisotropy of the tested foams. The cell ligaments were modeled as linearly elastic beams with Plateau border cross-sections that varied along their length in a manner observed in the foams tested. Accurate representation of these geometric characteristics was shown to be essential in the quantitative and qualitative success of the model.

The present study aims to use experiments to quantify the compressive response (e.g., Fig. 2) and understand the underlying mechanisms for Al alloy foams. Computed X-ray tomography is first used to characterize the microstructure and sub-

sequently to monitor the evolution of crushing in compression experiments. Part II presents idealized models based on suitably microstructured Kelvin cell domains that are used to reproduce the material compressive response and most of the associated events.

2. Foam morphology

Aluminum (Al-6101-T6) Duocel ® foams manufactured by ERG were used in this study. Their microstructures were analyzed using computed X-ray tomography. Three foams with nominal cell sizes of 10, 20 and 40 ppi were supplied in 4-in. (102 mm) thick blocks with planar dimensions of 12 × 14.5 in (305 × 368 mm). Their respective average relative densities were 8.23%, 7.50% and 7.54% (Table 1). The tomography system used is *Scanco Medical AG* Micro-CT-80 (μCT 80) with a maximum resolution of 10 μm. The most accurate rendering of the microstructure of our three foams was obtained by operating the facility at its highest resolution using specimens that did not exceed 18 mm in diameter. The facility was also used to monitor the evolution of crushing in specimens that were 51 mm^3 again operated at the maximum resolution. The images that will be presented were obtained using peak energy of 70 kVp and current intensity of 114 μA (for more on this, see Jang et al., 2008).

Duocel foam is thought to be made using polymeric foams as templates to generate a mold in which aluminum alloy is cast. On solidification, the mold material is removed leaving behind a replica of the original polymeric foam (see Section 2.5 in Ashby et al., 2000 and Zhou et al., 2005). By selecting the template foam it is possible to retain characteristics such as cell size uniformity exhibited by commercially available polymeric foams.

Fig. 1 shows a 3D tomography rendering consisting of a few cells from the 10 ppi foam. The cells are seen to be irregular polyhedra with nearly straight edges (ligaments). They are somewhat elongated in the vertical direction which we associate with the rise direction of the original polymeric template foam (henceforth called the "rise" direction for the Al foams also). The polyhedral geometry of cells is also illustrated in Fig. 3a, which shows individual cells extracted from the same foam. Fig. 3b shows a skeletal outline of the same cells formed by joining the centers of adjacent nodes with straight lines. The individual cell in the figure has 13 faces that include 3 quadrilaterals, 6 pentagons, 4 hexagons and a total of 33 ligaments. In the pair of cells, the one on the LHS has 14 faces with 4 quadrilaterals, 5 pentagons, 5 hexagons and a total of 36 ligaments while the one on the RHS has 12 faces with 2 quadrilaterals, 8 pentagons, 2 hexagons and a total of 30 ligaments (see also geometric characterization of similar foams in Perrot et al., 2007). As was the case for the PU foams of Gong et al. (2005), the general characteristics of the polyhedral microstructure is similar to that of Matzke's (1946) soap froth foam.

Images of this type were used to measure the cell size and the anisotropy. Cell size is defined by the average height of a cell in the rise direction $\bar{h}_1$ (see figure under Table 1). The range of cell sizes recorded was then used to establish a measure of *polydispersity* based on the ratio of one standard deviation (Σ_{h_1}) and the average cell height $\bar{h}_1$ (see Kraynik et al., 2004 for a

Table 1
Geometric parameters of Al-6101-T6 foams analyzed

Foam ppi	ρ^*/ρ (%)	$\bar{h}_1$ in (mm)	$h_1\|_{\min-\max}$ in (mm)	$\sum_{h_1}/\bar{h}_1$	λ	$\bar{\ell}$ in (mm)	$\sum_{\ell}/\bar{\ell}$	$\bar{A}_o \times 10^3$ in^2 (mm^2)	$\sum_{A_o}/\bar{A}_0$
10	8.23	0.184 (4.683)	0.158-0.234 (4.013-5.944)	0.0754	1.27	0.070 (1.780)	0.263	0.459 (0.296)	0.261
20	7.50	0.141 (3.570)	0.120-0.170 (3.048-4.318)	0.0707	1.24	0.048 (1.22)	0.277	0.144 (0.0929)	0.235
40	7.54	0.115 (2.929)	0.087-0.136 (2.210-3.454)	0.0749	1.18	0.041 (1.04)	0.268	0.0648 (0.0418)	0.238

ρ = 0.0972 lb/in^3 (2690 kg/m^3).

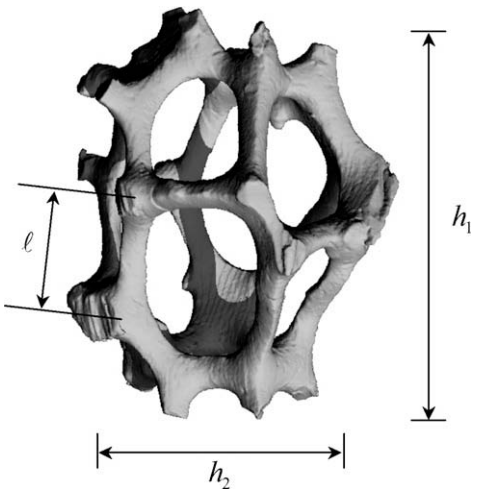

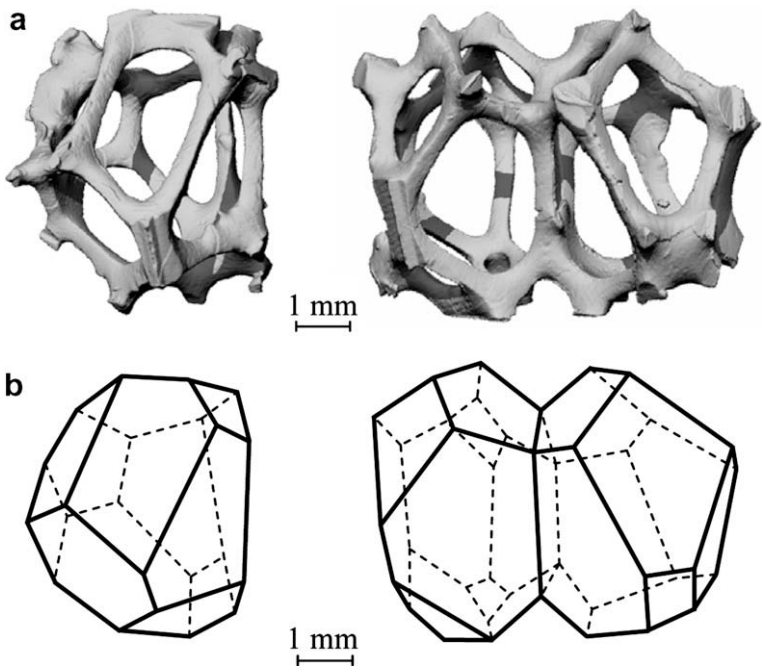

Fig. 3. Cells extracted from a 10 ppi Al foam illustrating irregular polyhedral geometry. (a) Tomography renderings and (b) skeletal drawings.

mathematically sharper definition of polydispersity). The results range from 0.071 to 0.075 indicating that cell size variation is small in this type of foam.

The cell dimensions in the transverse directions (h_2) were also measured and used to establish the anisotropy parameter $\lambda = h_1/h_2$. The mean values of measured λs reported in Table 1 vary from about 1.27 to 1.18 and decrease somewhat with decreasing cell size (Perrot et al., 2007, report somewhat higher values and a different trend in their anisotropy measurements on similar Duocel foams). These results are similar to those of polymeric foams reported in Huber and Gibson (1988), Gong et al. (2005) and Montminy et al. (2004) (the last reference used a more elaborate measure of anisotropy).

Micro-CT images were also used to establish the ligament length distributions for each of the three foams. The ligament length (ℓ) is defined as the distance between the centers of the nodes at the ends (see Fig. 4). The mean value of the measurements is listed in Table 1 under $\bar{\ell}$ while $\Sigma_\ell/\bar{\ell}$ is one standard deviation divided by the mean value. No significant difference was observed between the three foams (see also bar graph distribution of lengths in Fig. 10 in Jang et al., 2008).

The microstructures of the 10, 20 and 40 ppi foams are compared in Fig. 5. Micro-CT images assembled from the three foams have been scaled so that they appear to have about the same cell size. In this comparison, the foam microstructures

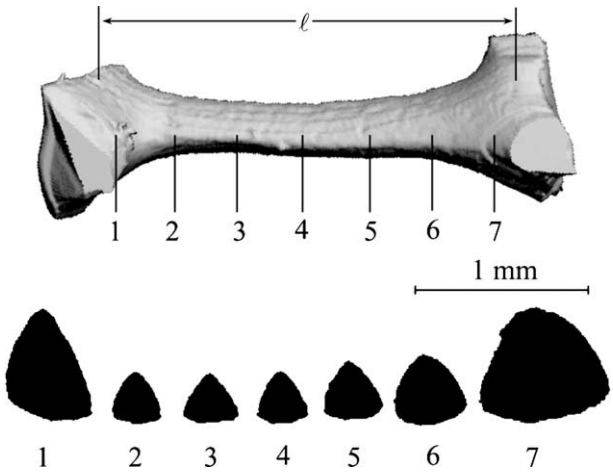

Fig. 4. Ligaments from a 10 ppi Al foam and cross-sectional views.

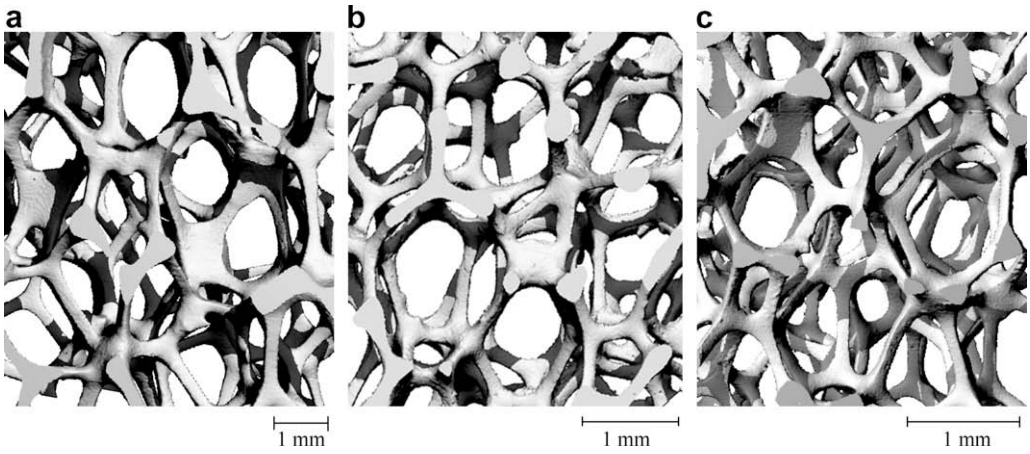

Fig. 5. Scaled images showing clusters of cells of foams of different cell sizes: (a) 10, (b) 20 and (c) 40 ppi.

are seen to be very similar. Since the foams have about the same density, it can be concluded that to first order the microstructure scales with cell size as indeed has been reported for polymeric foams Gong et al. (2005).

Gong et al. (2005) pointed out the importance of the variation of cross-sectional area of ligaments along their length on the mechanical properties. Area variation was found to be present in the Al foam ligaments although, as demonstrated in Fig. 4, the shapes of the cross-sections are distinctly different from those of polymeric foams. The concave, Plateau border shape that must have existed in the polymeric foam templates has been replaced by one with convex sides, resulting in a much bulkier ligament (similar results reported in Zhou et al., 2002). The nodes can be seen in Figs. 3 and 4 to have been similarly filled up as now they also have convex cross-sections. The net result of the bulkier construction of the ligaments and nodes is that the Al foams contain much more solid than their PU counterparts and consequently their relative density is much higher.

A large number of ligament images from the three foams were digitally sliced in the manner shown in Fig. 4 and the area of the cross-sections was calculated as a function of position. Fig. 6 shows a plot of the measured cross-sectional area $A(\xi)$ normalized by the value at mid-span, A_o, as a function of axial position, $\xi = x/\ell$. The data were fitted with the following symmetric function:

$$A(\xi) = A_o f(\xi) = A_o(36\xi^4 + \xi^2 + 1). \tag{1}$$

The micro-CT measurements showed that longer ligaments tend to have smaller A_o than shorter ones. Measured values of A_o are plotted against ligament length in Fig. 7. Each variable is normalized by the mean value of all the measurements ($\bar{A}_o$ and $\bar{\ell}$ given in Table 1). The following function for A_o was generated by fitting the data:

$$A_o(\eta) = \bar{A}_o g(\eta) = \bar{A}_o(0.6633 + 0.2648\eta^{-2.5963}), \quad \eta = \ell/\bar{\ell}. \tag{2}$$

The functions $f(\xi)$ and $g(\eta)$ will be used to define the ligament geometry in the analysis that follows in Part II.

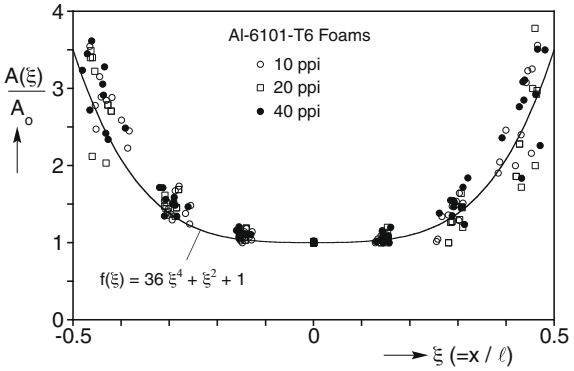

Fig. 6. Measured variation of Al foam ligament cross-sectional area along the length, fitted with function $f(\xi)$.

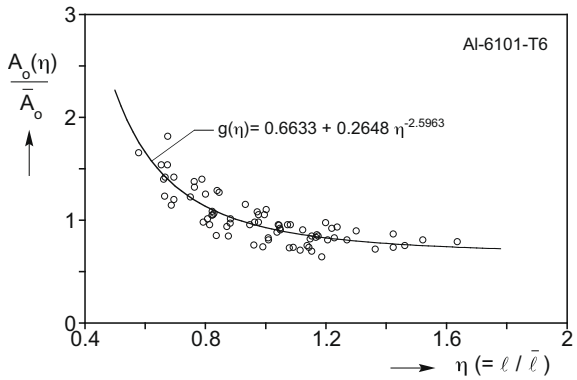

Fig. 7. Measured ligament mid-span cross-sectional area as a function of normalized ligament length fitted with function $g(\eta)$.

3. Compression and crushing experiments

Several compression tests were performed in the rise and transverse directions for each of the three foams. The specimens typically had a 2.0×2.0 in (51×51 mm) cross-section and a height of either 2.0 or 4.0 in (51 or 102 mm). They were extracted from the large blocks of foam supplied by the manufacturer using a computer operated wire EDM system. The process minimizes the distortion along the cut edges and provides a better parallelity between the two loaded surfaces. Furthermore, in order to minimize the influence of the edges on the initial response, Al-alloy plates were bonded to the two surfaces that were subsequently loaded as shown in Fig. 8 (plates 0.025 in thick; adhesive film 3M-AF163-2). The specimens were compressed between parallel platens in a stiff electromechanical testing machine run under displacement control. The typical displacement rate was $\dot{\delta}/H = 8.3 \times 10^{-4}\ \mathrm{s}^{-1}$ (corresponds to the strain rate when the deformation is homogeneous; H is the height of the specimen). Small variations in density were found to be present in the foam blocks and consequently the relative densities of individual specimens reported in Tables 2 and 3 differ to some degree from the average values listed in Table 1.

The specimen cross-section was selected to be 2.0 in as this was the largest size that could be scanned in our micro-CT. Two inches encompasses about 80, 40 and 20 cells, respectively, for the 40, 20 and 10 ppi foams. Previous experience with cellular materials has taught that 20 cells across may have been somewhat small, at least for elastic properties. Thus, the effect of specimen width on the results was evaluated by comparing results from specimens of increasing size. It was found that the biggest influence of specimen size was in the initial elastic properties measured whereas the effect on the rest of the response was too small to establish (see also Sections 2.3 and 4.4 in Papka and Kyriakides, 1998a). However, small imper-

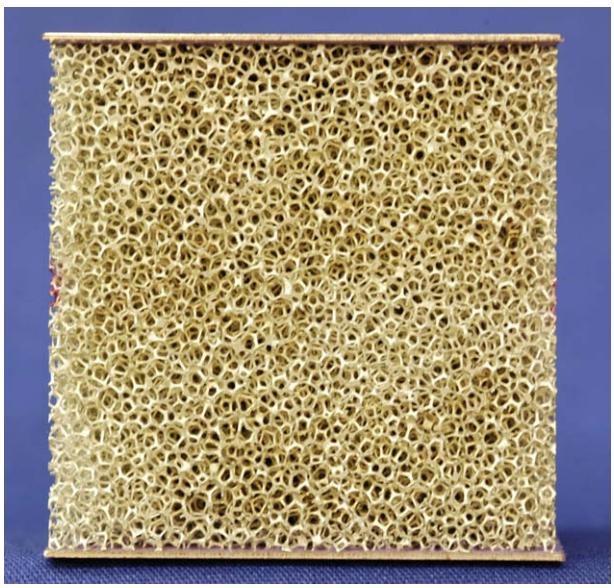

Fig. 8. Photograph showing a typical specimen used in compression experiments.

Table 2
Measured mechanical properties of A1-6101-T6 foams in the rise direction

Exp. no.	ρ^*/ρ (%)	E_1^*/E (%)	σ_{I1} psi (MPa)	$\bar{\sigma}_{P1}$ psi (MPa)	$\Delta\varepsilon_{P1}$ (%)
(a) 10 ppi, λ = 1.27					
R10-1	8.33	0.865	396 (2.73)	–	–
R10-2	8.79	0.857	456 (3.14)	431 (2.97)	49
R10-3	8.63	0.863	446 (3.08)	424 (2.92)	46
R10-4	8.48	0.871	396 (2.73)	384 (2.65)	48
(b) 20 ppi, λ = 1.24					
R20-1	8.26	0.705	352 (2.43)	–	–
R20-2	7.47	0.677	283 (1.95)	–	–
R20-3	8.43	0.779	379 (2.61)	362 (2.50)	49
R20-4	8.37	0.857	369 (2.54)	357 (2.46)	49
(c) 40 ppi, λ = 1.18					
R40-1	7.98	0.660	339 (2.34)	–	–
R40-2	8.20	0.746	360 (2.48)	363 (2.50)	49
R40-3	8.24	0.780	393 (2.71)	390 (2.69)	52
R40-4	8.18	0.733	406 (2.80)	400 (2.76)	51

$E = 10^4$ ksi (69 GPa), $\nu = 0.3$.

Table 3
Measured mechanical properties of A1-6101-T6 foams in the transverse direction

Exp. no.	ρ^*/ρ (%)	E_2^*/E (%)	σ_{I2} psi (MPa)	$\bar{\sigma}_{P2}$ psi (MPa)	$\Delta\varepsilon_{P2}$ (%)
(a) 10 ppi, λ = 1.27					
T10-1	8.56	0.466	290 (2.00)	289 (1.99)	38
T10-2	8.48	0.493	298 (2.05)	295 (2.03)	38
T10-3	8.74	0.527	333 (2.30)	324 (2.23)	39
(b) 20 ppi, λ = 1.24					
T20-1	7.36	0.459	297 (2.05)	–	–
T20-2	7.67	0.426	308 (2.12)	317 (2.19)	39
T20-3	7.70	0.479	309 (2.13)	319 (2.20)	38
(c) 40 ppi, λ = 1.18					
T40-1	8.22	0.570	294 (2.03)	320 (2.21)	[a]
T40-2	8.03	0.506	323 (2.23)	331 (2.28)	40
T40-3	8.03	0.538	289 (1.99)	315 (2.17)	[a]

$E = 10^4$ ksi (69 GPa), $\nu = 0.3$.
[a] Nearly monotonic response.

fections in the experimental set up such as non-perfect parallelity of the loaded surfaces had an even larger effect on the initial modulus. The influence of such effects was minimized by unloading the specimen to some degree soon after the first load peak and measuring the elastic modulus from the linear unloaded response as shown in Fig. 2.

3.1. Compressive response in rise direction

The main characteristics of the material response in the rise direction and the associated events will be demonstrated through an example involving a test on a 10 ppi foam specimen. In this particular case the specimen was crushed in increments of δ/H of about 4–5%. After each crushing increment the specimen was unloaded, removed from the testing machine, placed in the micro-CT and scanned. The Al-alloy foam deformed plastically during crushing and this enabled us to follow the evolution of plastic deformation in the specimen. Crushing was taken to δ/H of about 55% and fourteen full-scale 3D images of the specimen at various degrees of crushing were recorded in the course of the test. Fig. 9 shows the recorded stress–displacement response where the linear unloading and reloading paths have been truncated for clarity (rise direction compressive responses on similar Al foams but annealed 6101 alloy appeared in Zhou et al., 2004 and Zhou and Soboyejo, 2004). Fig. 10 shows the initial and five deformed images of internal planar views of the whole specimen (the images are 0.35 in (9 mm) from one of the edges). The configurations correspond to locations on the response marked with numbers inside square boxes (atop of the response). (Bart-Smith et al., 1998 used X-ray tomography to capture details of cell deformation in open and closed cell metallic foams.)

The evolution of crushing will be monitored in more detail using expanded images of two 20 × 20 mm sites in the same plane. Sites A and B are marked with yellow boxes in the undeformed configuration in Fig. 10 (⓪). Eight images of these sites that correspond to the unloading positions marked on the response in Fig. 9 with numbers in circles (below the response) appear in Figs. 11 and 12. (Gioux et al., 2000 presented good quality micro-CT images of Duocel showing ligament deformation during the initial stable part of the response under hydrostatic pressure.)

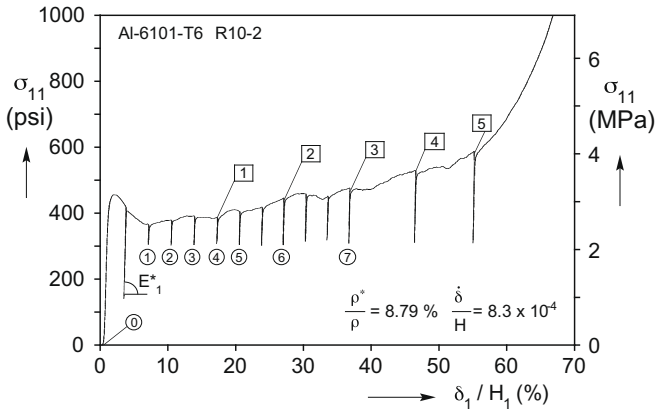

Fig. 9. Rise direction compressive response for specimen R10-2.

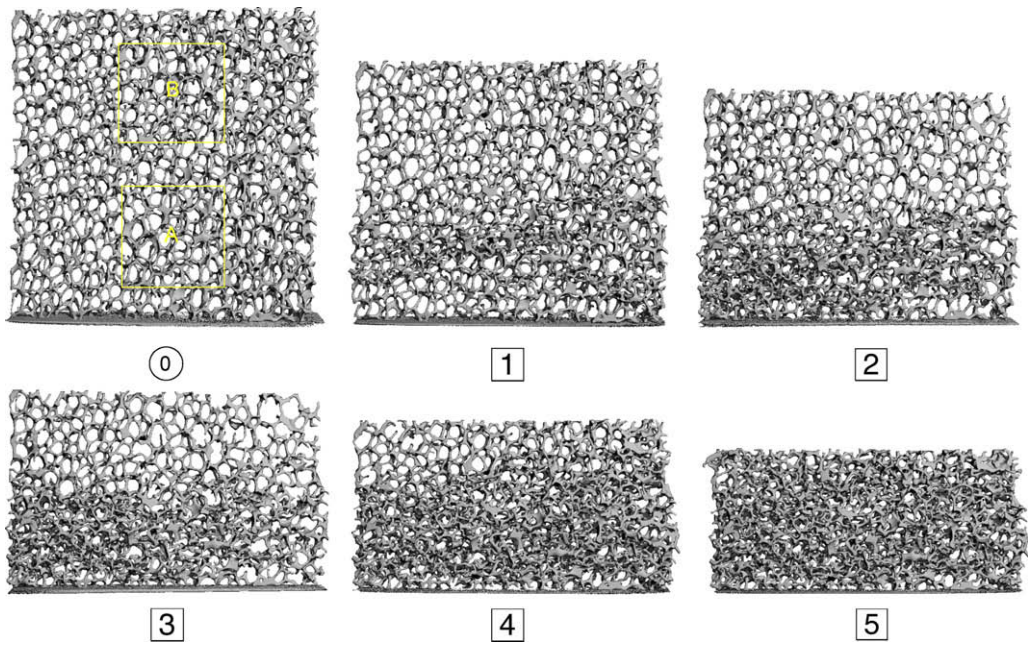

Fig. 10. Sequence of full cross-section deformed configurations corresponding to points ⓪ and 1 to 5 on response in Fig. 9.

In an effort to show how crushing evolved through the rest of the specimen, Fig. 13 shows 3D images of two perpendicular internal planes corresponding to points 1 to 2 on the response. In the undeformed block the two internal planes were approximately 0.35 in (9 mm) from the corresponding free surfaces. For better clarity each image corresponds to a thin slice of the material (~9 mm thick).

Several small salt (sodium metatungstate) markers placed on one of the faces of the specimen were used as guides to generate an x–y–z coordinate for each scan. The salt markers have a different density than Al and are thus distinguished by X-rays. This coordinate system is used to return to approximately the same location after each 3D image is assembled. However, two factors make returning exactly to the same plane after each loading somewhat difficult. First, after each unloading the specimen is reinstalled in the micro-CT at a slightly different position. Second, the specimen is getting progressively more deformed. The combined effect is that the coordinate system gets one close to the desired site, but the final position of the plane is chosen manually by matching local geometric features. Thus, although the thickness of the images is selected to be the same in each case, the positions of the front and back planes differ slightly from one image to another. This is responsible for small differences observed between images particularly at site B in Fig. 12.

Returning to the response in Fig. 9, it is seen to exhibit an initial linear regime that terminates in a local load maximum at a stress of $\sigma_{l1} = 456$ psi (3.14 MPa). During the linear part of the response the specimen deformation is macroscopically

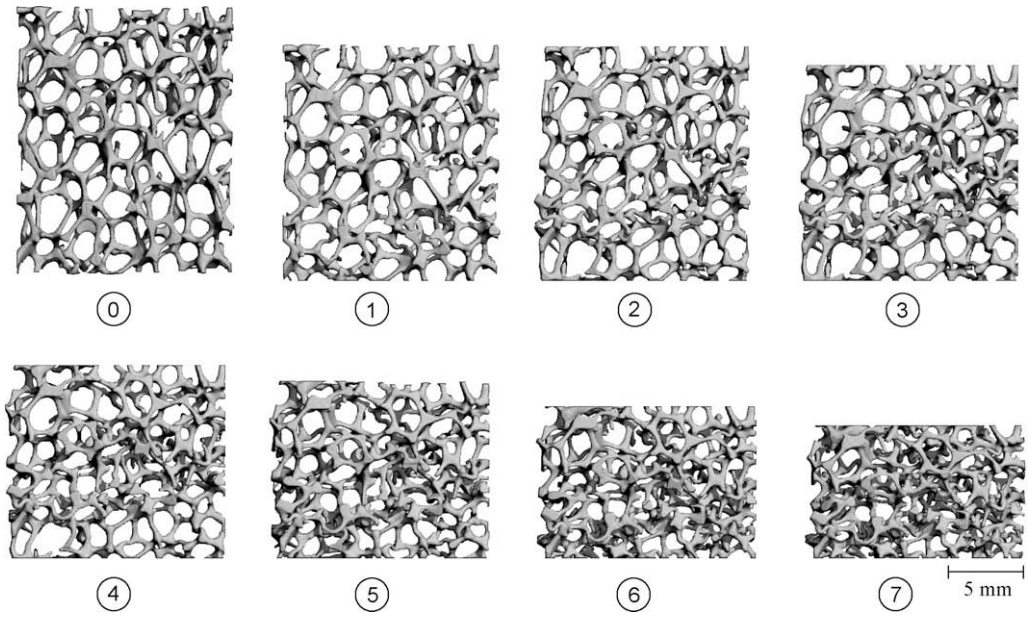

Fig. 11. Sequence of deformed configurations of site A corresponding to points ⓪ to ⑦ on response in Fig. 9 (site A marked with yellow box in configuration ⓪ in Fig. 10).

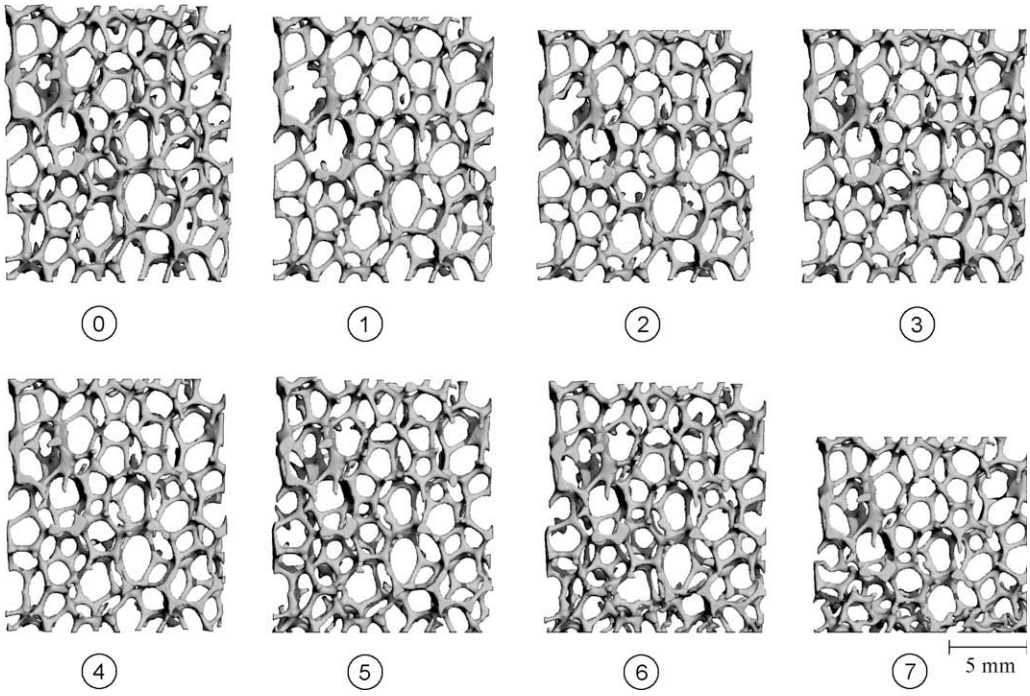

Fig. 12. Sequence of deformed configurations of site B corresponding to points ⓪ to ⑦ on response in Fig. 9 (site B marked with yellow box in configuration ⓪ in Fig. 10).

homogeneous. The limit load is a sign that localization of deformation has commenced somewhere within the specimen. The elastic modulus of the foam was measured from the first unloading and found to be $E_1^* = 8.57E \times 10^{-3}$ (E is the elastic modulus of bulk Al-6101-T6). The response drops down to a local minimum close to the second unloading position and then traces a somewhat ragged plateau. Images ① in Figs. 11 and 12 were taken after the second unloading. Signs of local liga-

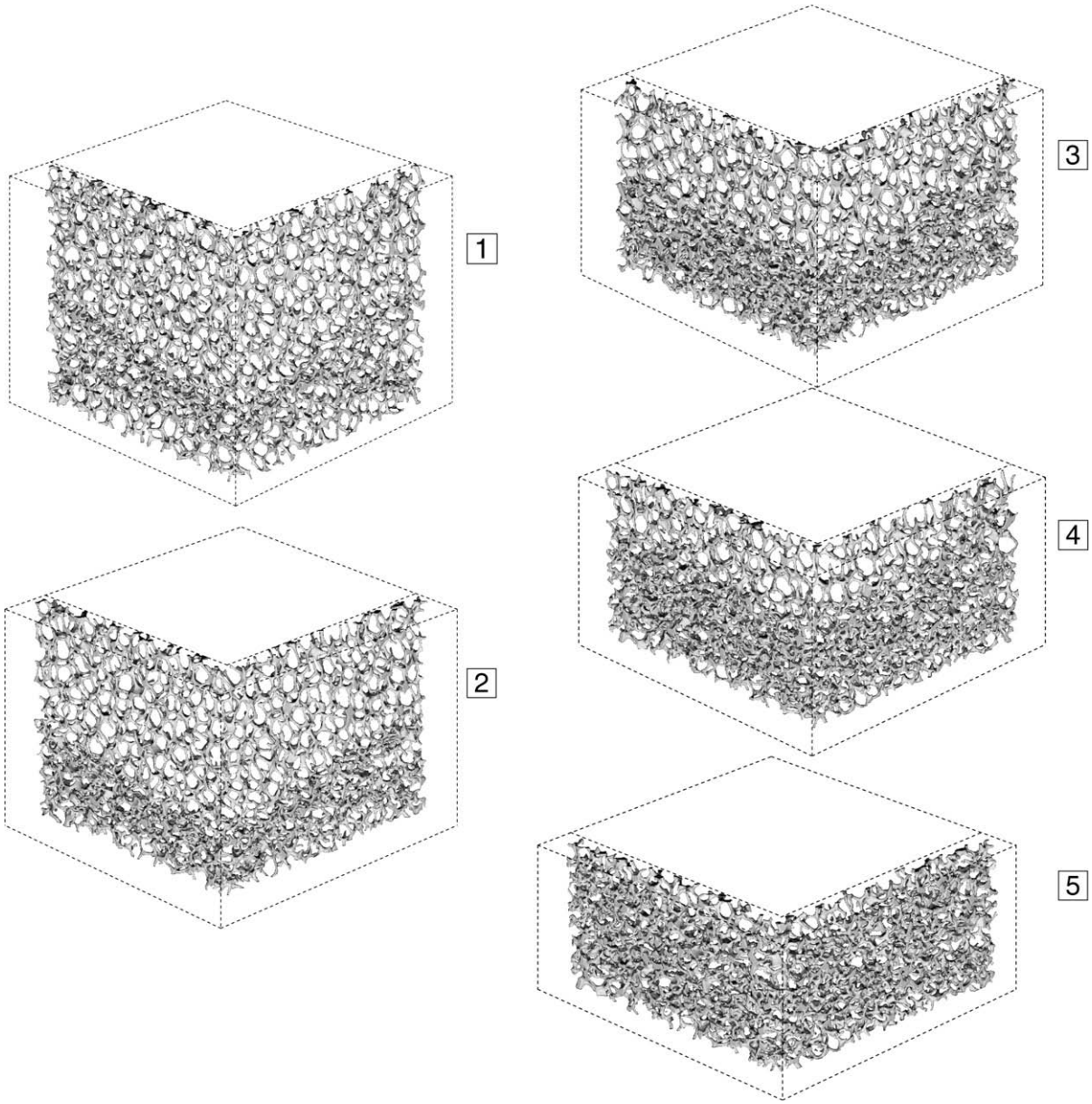

Fig. 13. Sequence of 3D images of two perpendicular planes corresponding to points 1 to 5 on response in Fig. 9.

ment buckling are clearly seen in the lower right-hand side of the image at site A whereas at site B the microstructure remains unaffected. By configuration ② a clear band of crushed cells is seen to cross the image at site A; in image ③ the crushing has spread upwards widening the band to about four cells. In image ④ the band has spread further upwards and collapsed cells now cover most of the central two thirds of this domain. Simultaneously the corresponding images at site B remain totally unaffected and look the same as the initial image.

A more global view of what had taken place can be seen in the full specimen images 1 in Figs. 10 and 13, which correspond to images ④ in Figs. 11 and 12. In Fig. 10, an inclined band of crushed material crosses the specimen from left to right. This is met around mid-width by a second band that emanated from the lower right-hand corner of the specimen. At the same time, image 1 in Fig. 13 shows that the crushing zones had a 3D distribution in the specimen, as the crushed band is also inclined in a plane perpendicular to the original one. Furthermore, images taken at different depths through the specimen showed the crushing not to be planar. As mentioned earlier, small differences in density were observed through the specimens especially when they originated close to the edges of the original block. Such inhomogeneities are thought to be responsible for the complexity of the initial crushing zones in this specimen and for the unusual raggedness of this particular response.

At higher values of δ/H the crushing is seen to spread further in region A as illustrated in images ⑤ and ⑥ in Fig. 11. By configuration ⑦ the whole of this region has crushed. By configuration ⑤ in Fig. 12 the collapse front is seen to have reached the very bottom of region B where a couple of cells are starting to collapse while most of the region above remains intact. In configurations ⑥ a band of collapsed cells extends across this site and by ⑦ the whole lower end is crushed.

As evidenced by the global images in Figs. 10 and 13, cell collapse did not start from the ends but rather along inclined bands approximately at one third of the height of the specimen above the lower faceplate. Furthermore, the crushing surface was not planar. By configuration 2 the crushing has consumed the lower one-third of the specimen with a few cells bonded to the faceplate remaining intact. By configuration 3 the crushing has consumed the lower 60% of the specimen and the crushing front is now more planar and nearly parallel to the faceplates. The crushing front continues to move upwards (see image 4) but with a gradual increase in the load. The last image (5) was taken at $\delta/H = 55\%$ and as can be seen most of the cells have crushed with a few bonded to the two faceplates remaining intact. Consequently, further compression requires an increasingly higher load as the material is now in the densified regime.

In summary then, following the initial load maximum a band of cells started to collapse. The band is inclined, is not planar and is away from the top and bottom ends where cells were slightly reinforced by bonding to thin plates. As loading progresses destabilized cells at the interface between collapsed and intact cells collapse next and in this manner the band broadens with the load remaining nearly constant. Crushing spread to the lower part of the specimen first, with relatively modest increase in the load. Subsequently, the crushing front propagated upwards but this required a gradual increase in the load. As will be seen below in results from other experiments, this increase in the load was unusual and is attributed to small density inhomogeneities in this particular specimen.

This sequence of events is reminiscent of that reported in Papka and Kyriakides in the case of in-plane crushing of polymeric (1998a) and metallic honeycombs (1994, 1998b). By contrast, in similar compression tests on polyester urethane foams that are essentially elastic, Gong and Kyriakides (2005) noted that crushing was initiated by a long-wave buckling mode that affected the whole specimen and subsequently lead to the formation of many localized bands of crushed cells. Clearly, no long-wave buckling was observed in the Al foam test described here and the crushing spread mainly by the propagation of two crush fronts.

Twelve such experiments, four for each of the three foams analyzed, were conducted and the results are summarized in Table 2. As mentioned earlier, small variations in density were observed in each block and thus the average density of each individual specimen is seen to be different. Although small variations in anisotropy were also observed, establishing the value of λ for each specimen was not pursued and so the average value for the whole block is reported instead. Listed are the elastic moduli (E_1^*), the crushing initiation stresses (σ_{I1}), the plateau stresses ($\bar{\sigma}_{P1}$) and the extent of the plateau ($\Delta\varepsilon_{P1}$). $\bar{\sigma}_{P1}$ is defined as the average stress of the response from its lowest point right after the initiation peak, to a value 1.4 times higher on the ascending branch at the end. $\Delta\varepsilon_{P1}$ is the average strain from the initiation peak to this stress value on the ascending branch.

The measured elastic moduli are plotted against the relative density in Fig. 14a and are seen to fall along a nearly linear trajectory. The degree to which they deviate from linearity is mainly attributed to variations in anisotropy. The initiation and propagation stresses are also plotted against relative density in Fig. 14b. As evidenced by the numbers in Table 2, for each case the two stresses are reasonably close to each other with $\bar{\sigma}_{P1}$ being somewhat lower. Once again, for the limited range of relative densities considered, the two stresses can be said to vary essentially linearly with relative density (Nieh et al., 2000) have presented similar order of magnitude result for E_1^* and σ_{I1} for Duocel foams of relative densities of about 9.2%). In all the tests the $\Delta\varepsilon_{P1}$ defined as mentioned above was approximately 50%. Finally, Fig. 15 compares the complete responses from specimens of 10, 20 and 40 ppi. The three specimens were chosen to have values of relative density that are close to each other. Consequently, the three responses are seen to be very similar to each other.

3.2. Compressive response in transverse direction

A similar series of tests was performed for specimens prepared in the same manner but loaded in the transverse direction. A representative set of results that appear in Figs. 16–20 (Exp. T10-1) will be used to outline the observed behavior. Fig. 16 shows the measured stress–displacement response, which was interrupted twelve times to allow scanning of the specimen. Global scans of an internal plane appear in Fig. 17 and more detailed images of two sites marked in yellow boxes in the undeformed configuration (⓪) appear in Figs. 18 (site A) and 19 (site B). The images correspond to the numbers in circles in Fig. 16 that identify the positions at which the response was unloaded. Fig. 20 shows the evolution of crushing on two internal perpendicular planes at the positions on the response (Fig. 16) marked with numbers in square boxes.

The response is similar to ones recorded in the rise direction. It exhibits a small initial load peak following which (①) ligament buckling is seen to start approximately in the middle of site A. In configuration ② several cells are seen to collapse and by configuration ③ a crushed zone of cells runs across this zone. At the same time, the corresponding images at site B remain unaffected. The global images 1 in Figs. 17 and 20 show once more a crushing band to have developed in the lower part of the specimen. The crushing follows a surface with a 3D relief. Subsequently crushing has initiated further up in the specimen as evidenced by global configurations 2. The crushing is seen in ④ to have reached the lower end of site B while it seems first to have slowed down and, in the corresponding image at site A, ceased. Global images 3 and 4 show that in this case several inclined crushing zones have developed through the specimen despite the fact that the load has remained relatively unchanged. By configuration 5 most of the cells have collapsed and the load required for further deformation has

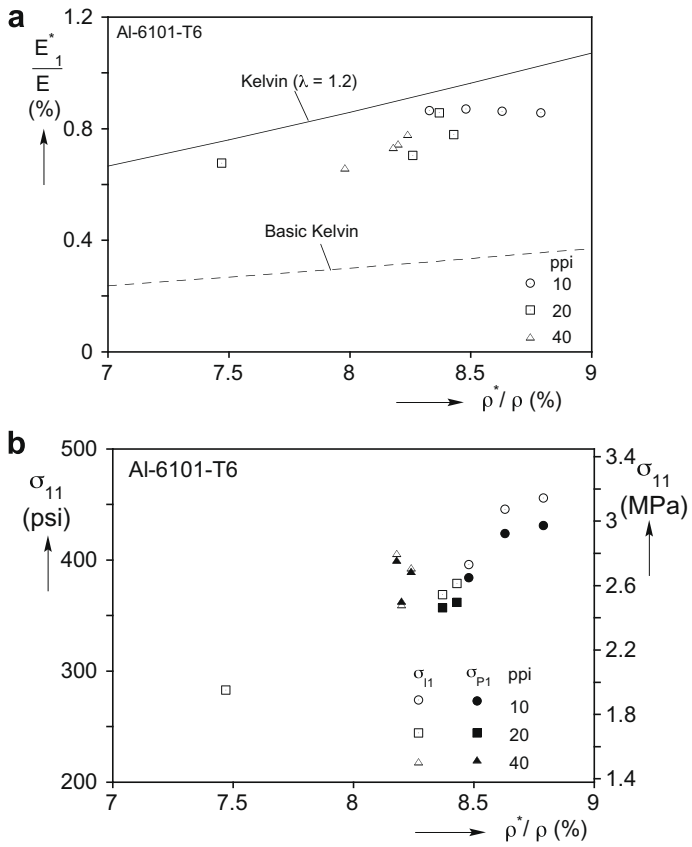

Fig. 14. Measured rise direction material parameters: (a) elastic modulus E_1^*/E and (b) initiation stress σ_{I1} and stress plateau $\bar{\sigma}_{P1}$. Included in (a) are predictions of the modulus based on the Kelvin cell model of Jang et al. (2008). The predictions from the "basic Kelvin" cell are discussed in Section 3.1 of Part II.

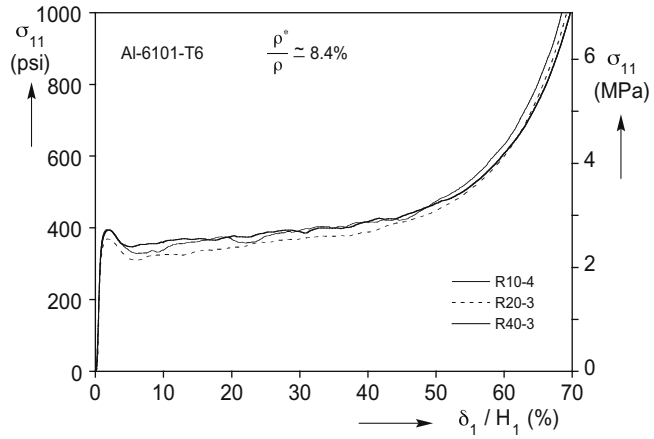

Fig. 15. Comparison of rise direction compressive responses from specimens of different cell sizes.

started to increase. It is noteworthy that in this case a number of cells dispersed throughout the specimen remain intact. These will crush subsequently at a higher load.

Nine crushing tests, three for each foam, were performed in the transverse direction and the main parameters of the responses are listed in Table 3. The elastic moduli (E_2^*) are plotted against density in Fig. 21a and are seen to vary approximately linearly with ρ^*/ρ. The three points from the 10 ppi foam fall somewhat lower, an indication that the 20 cell specimen size may have been a bit too small. The initiation and propagation stresses are plotted in Fig. 21b against density

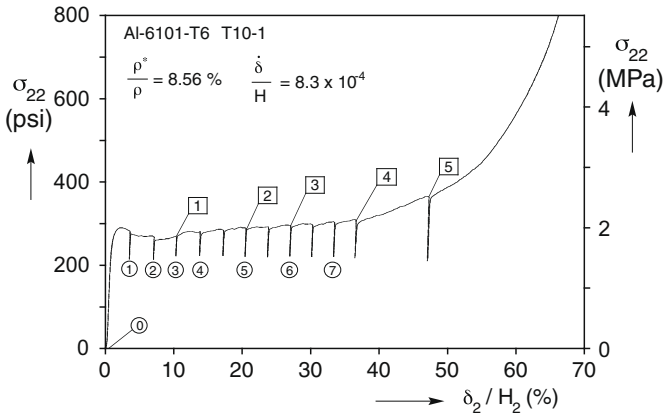

Fig. 16. Transverse direction compressive response for specimen T10-1.

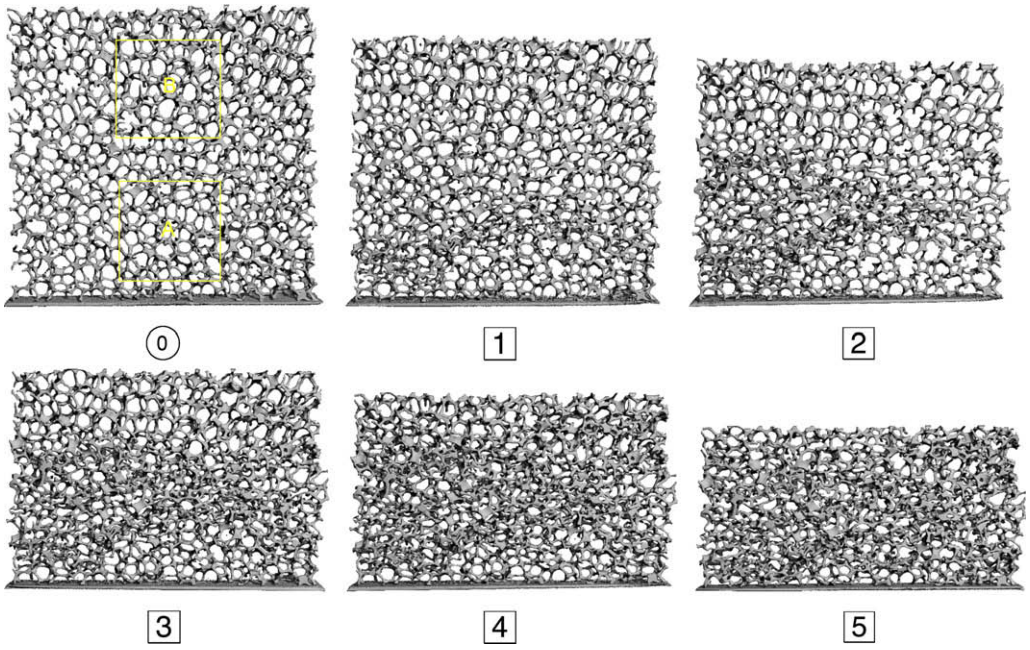

Fig. 17. Sequence of full cross-section deformed configurations corresponding to points ⓪ and 1 to 5 on response in Fig. 16.

(see also Nieh et al., 2000). A general observation from these tests was that the initiation peak was relatively small. In fact, for the 40 ppi foam, it is barely distinguishable and for two of the responses the stress exhibits a continuous small increase after the stress peak. For this reason $\bar{\sigma}_{P2}$ was defined somewhat differently from $\bar{\sigma}_{P1}$. Because of the smaller initiation peak, in this case the end of the plateau was assumed to be at 1.2 times the lowest stress in the response, which typically occurs just after the initiation stress peak. Despite this difference, for several of the specimens σ_{I2} is seen to be somewhat smaller than $\bar{\sigma}_{P2}$ which is rather unorthodox. In addition, the extent of the plateau is now approximately 38%. The two 40 ppi cases with nearly a monotonic response register 26% according to this measure which is misleading and as a result these values are not included in Table 3.

Transverse responses from the three foams analyzed are compared in Fig. 22. The three cases were selected to have relative densities as close to 8.0% as possible. The three responses follow similar trajectories with somewhat different stress levels primarily because of some differences in anisotropy and in relative density.

It is interesting to compare the present transverse responses with those from the polyester urethane foams of Gong et al. (2005). Polyester urethane is essentially an elastic material while the foams exhibited slightly higher anisotropies than the present foams. Unlike the response in the rise direction, the transverse response was essentially monotonic indicating that cell crushing was in effect randomly distributed. Al plasticity has introduced a limit load and localization of crushing fol-

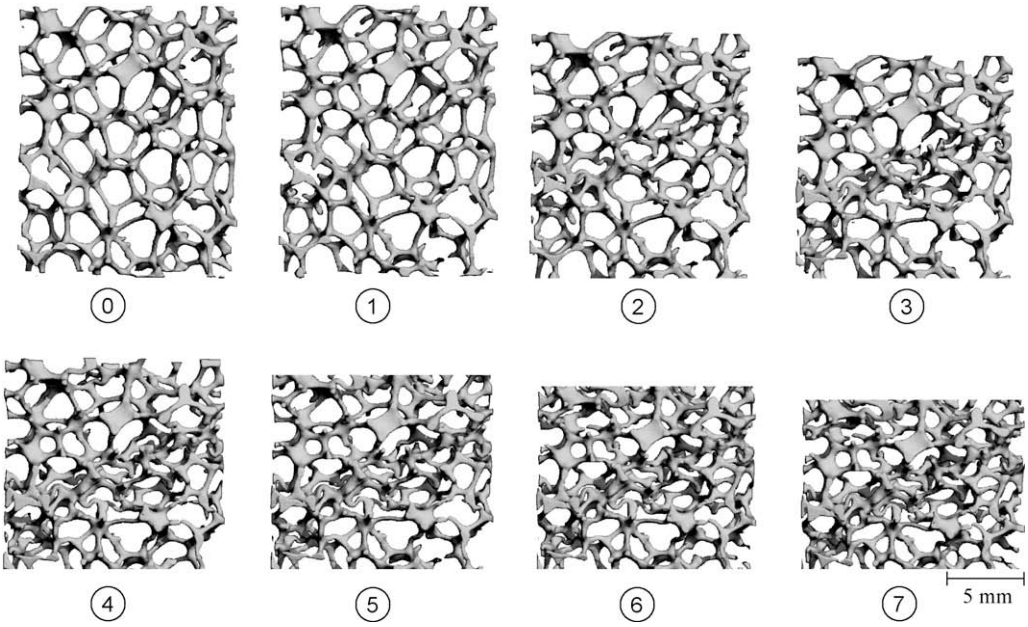

Fig. 18. Sequence of deformed configurations of site A corresponding to points ⓪ to ⑦ on response in Fig. 16 (site A marked with yellow box in configuration ⓪ in Fig. 17).

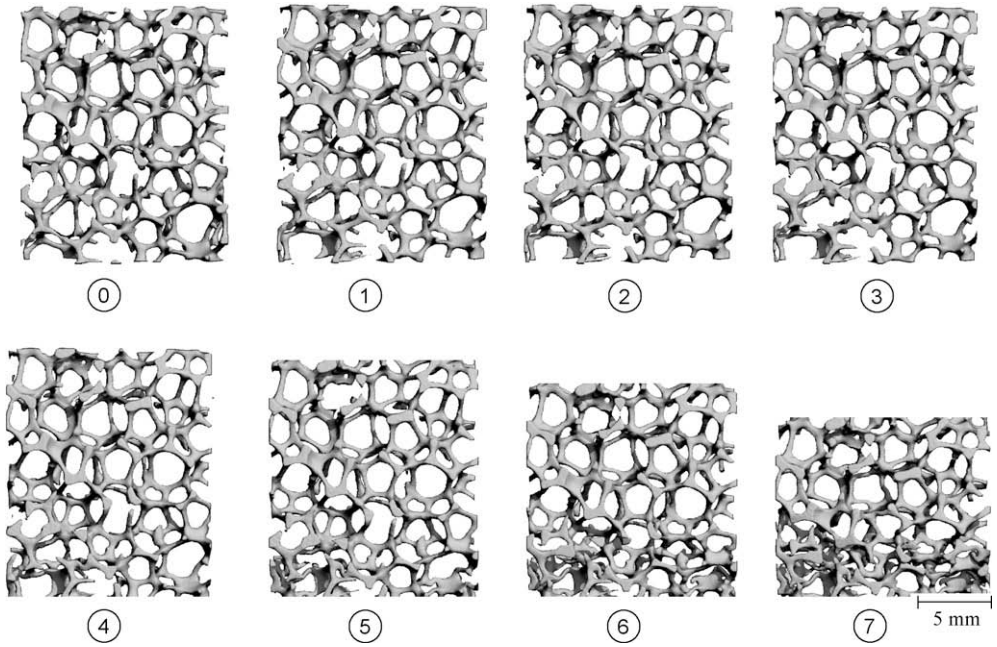

Fig. 19. Sequence of deformed configurations of site B corresponding to points ⓪ to ⑦ on response in Fig. 16 (site B marked with yellow box in configuration ⓪ in Fig. 17).

lowed by spreading at a nearly constant load. In other words, in the presence of plasticity the responses and associated events are similar in the two directions. The anisotropy makes the moduli in the rise direction higher, the initiation stress peaks more distinct and the stress plateaus higher than in the transverse direction as illustrated from the comparison of two different direction responses in Fig. 23 for our 10 ppi foam.

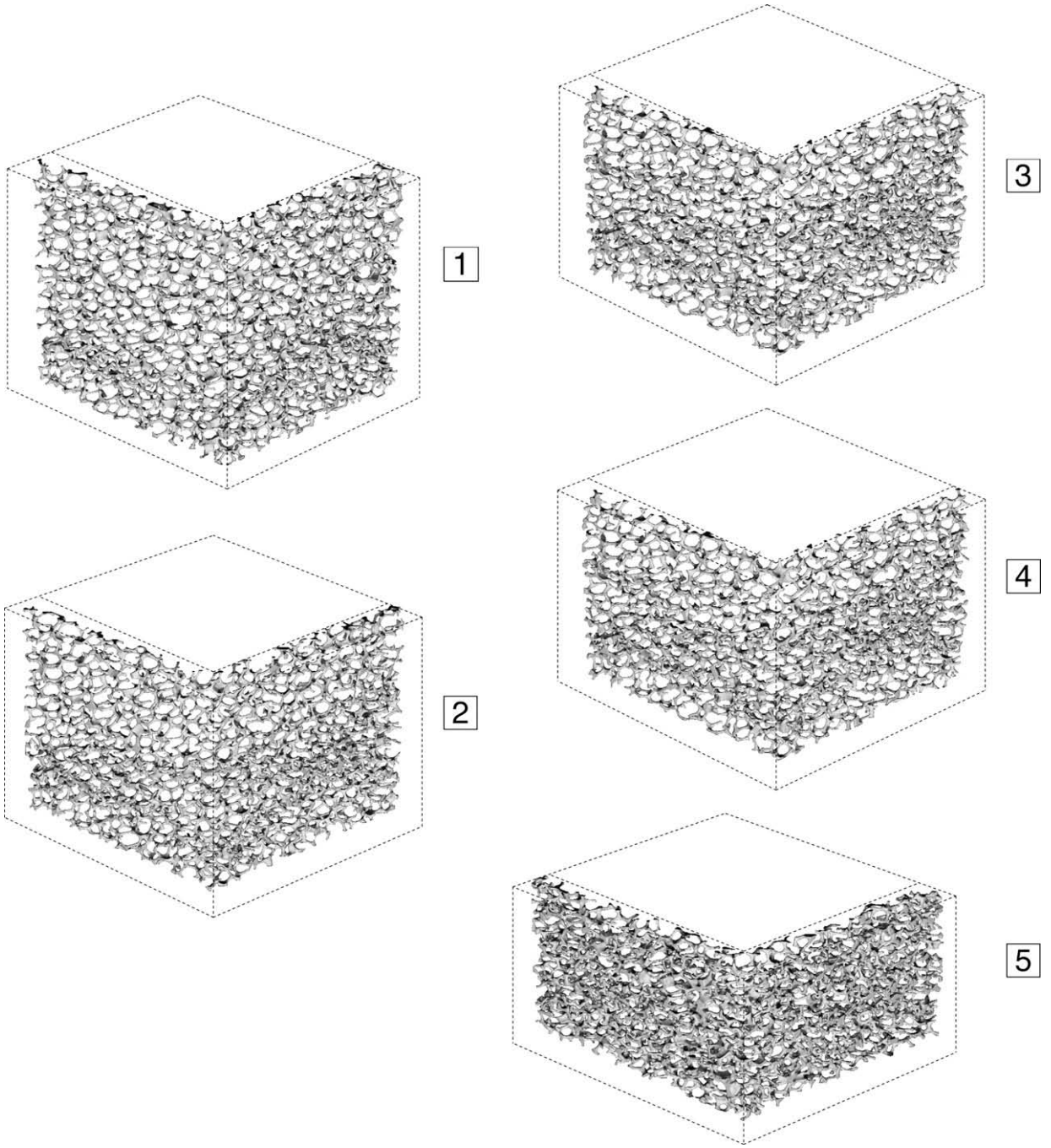

Fig. 20. Sequence of 3D images of two perpendicular planes corresponding to points 1 to 5 on response in Fig. 16.

4. Summary and conclusions

This two-part study has been concerned with the understanding of the response of Al-6101-T6 alloy open-cell foams (*Duocel* ®) to uniaxial compression. Part I first uses X-ray tomography to characterize the cell and ligament morphology. Foams of 10, 20 and 40 ppi with a relative density (ρ^*/ρ) in the range of 7.50–8.23% were analyzed. The microstructure consists of irregular polyhedra, with about the same number of faces and types of polygons as those reported by Matzke (1946) for soap froth (i.e., average number of faces of approximately 13.7, each face having an average of nearly five sides). In these foams the size of the cells does not vary significantly and the three microstructures were found to scale with cell size (to a

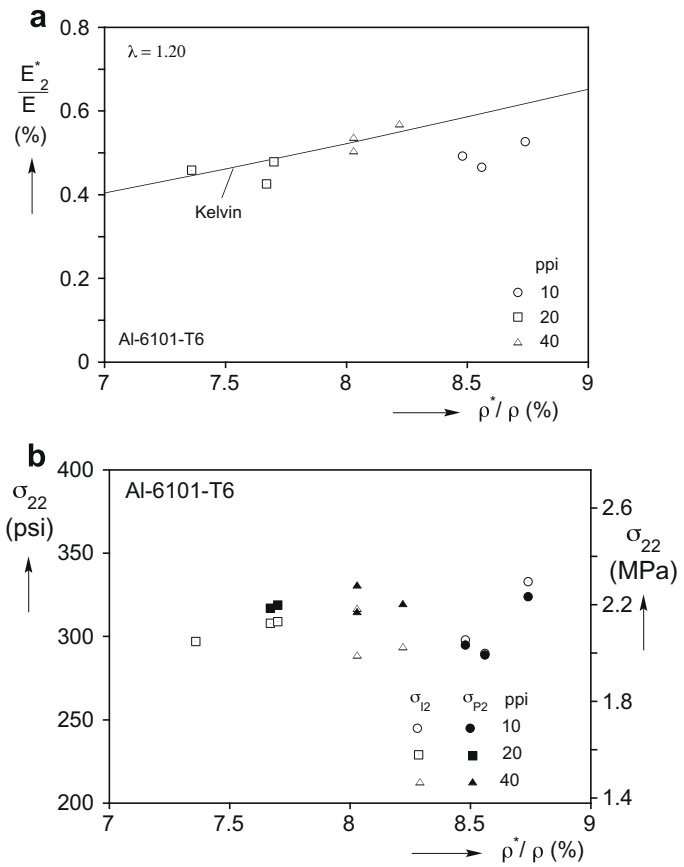

Fig. 21. Measured transverse direction material parameters: (a) Elastic modulus E_2^*/E and (b) initiation stress σ_{I2} and stress plateau $\bar{\sigma}_{P2}$.

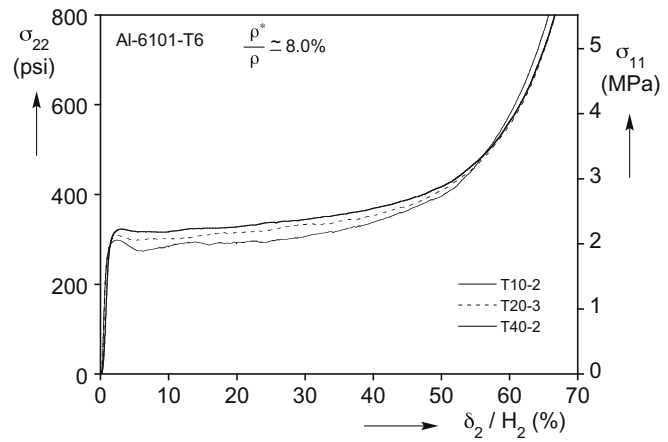

Fig. 22. Comparison of transverse direction compressive responses from specimens of different cell sizes.

first order approximation). The cells are elongated in one direction exhibiting anisotropies in the range of 1.18–1.27. Unlike polymeric foams, the Al foam ligaments were found to have rounded convex cross sections that were somewhere between equilateral triangles and circles with a variable area distribution along the length. The ligament area distribution was established from multiple measurements and approximated by a symmetric function (1). The mid-span cross-sectional area was found to depend on the ligament length and this was also quantified experimentally (fitted with Eq. (2)). The aluminum alloy of the base material exhibits the usual elastoplastic behavior with a modulus of 10^4 ksi (69 GPa) and yield stress of 28.3 ksi (195 MPa).

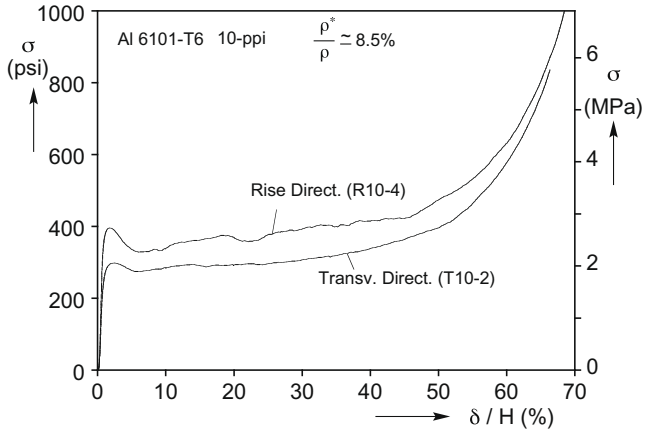

Fig. 23. Comparison of compressive responses in rise and transverse directions.

Cubical specimens (51 mm^3) extracted from the three foams were compressed between rigid plates at slow, constant displacement rates. Tests were performed along the rise and transverse directions after bonding thin plates to the compressed sides. The evolution of crushing in the specimens was monitored using X-ray tomography. In both directions, the foams exhibit a force–displacement response shared with many other cellular materials. It starts with a nearly linear elastic regime, which terminates into a limit load that is followed by an extensive load plateau. During the initial essentially elastic regime the specimen deformation is macroscopically uniform. Combined compression and bending of the ligaments eventually causes plastification and a gradual reduction of the foam stiffness leading to a limit load. Following the limit load, cells start to buckle and collapse locally, forming a band(s) that covers the whole cross-section of the specimen. The initial bands have a three-dimensional relief that generally is at an angle to the direction of loading. However, no prevalent band orientations were detected. Local deformation is arrested when ligaments of the collapsing cells come into contact. This triggers collapse in neighboring cells and in this manner crushing gradually spreads throughout the specimen while the load remains nearly constant (or experiences a gradual increase because of inhomogeneities in the microstructure). When most of the cells are thus crushed, the response gradually stiffens. Compression along the transverse direction produces a similar response with a lower elastic modulus, and somewhat lower limit and plateau stresses than the corresponding values in the rise direction.

Several crushing experiments have been performed on each of the three different size foams and the major parameters of the material responses have been recorded. These parameters along with the qualitative features of the crushing will form the basis for evaluating the performance of models developed in Part II of this study.

Acknowledgements

The authors acknowledge with thanks the financial support of the work by the National Science Foundation through Grant CMS-0527906. The authors wish to thank B.D. Leyda and ERG for providing the Duocel aluminum foam samples used in the study to our specifications. We are also grateful to Scanco engineers for their support in multiple ways in the use of our micro-CT-80 system and to Richard Ketcham for his insightful tutorials on X-ray tomography. Finally we are thankful to Lixin Gong for his help in many ways offered in the course of this study.

References

Ashby, M.F., Evans, A., Fleck, N.A., Gibson, L.J., Hutchinson, J.W., Wadley, H.N.G., 2000. Metal Foams: A Design Guide. Butterworth-Heinemann.
Bart-Smith, H., Bastawros, A.-F., Mumm, D.R., Evans, A.G., Sypeck, D.J., Wadley, H.N.G., 1998. Compressive deformation and yielding mechanisms in cellular Al alloys determined using X-ray tomography and surface strain mapping. Acta Mater. 46, 3583–3592.
Gibson, L.J., Ashby, M.F., 1997. Cellular Solids: Structure and Properties, 2nd ed. Cambridge University Press, Cambridge.
Gibson, L.J. (Ed.), 2003. Cellular solids. MRS Bull. (4).
Gioux, G., McCormack, T.M., Gibson, L.J., 2000. Failure of aluminum foams under multiaxial loads. Int. J. Mech. Sci. 42, 1097–1117.
Gong, L., Kyriakides, S., Jang, W.-Y., 2005. Compressive response of open-cell foams. Part I: Morphology and elastic properties. Int. J. Solids Struct. 42, 1355–1379.
Gong, L., Kyriakides, S., 2005. Compressive response of open cell foams. Part II: Initiation and evolution of crushing. Int. J. Solids Struct. 42, 1381–1399.
Hilyard, N.C., Cunningham, A. (Eds.), 1994. Low Density Cellular Plastics: Physical Basis of Behaviour. Chapman & Hall, London.
Huber, A.T., Gibson, L.J., 1988. Anisotropy in foams. J. Mater. Sci. 23, 3031–3040.
Jang, W.-Y., Kyriakides, S., Kraynik, A.M., 2008. On the microstructure of open-cell foams and its effect on elastic properties. Int. J. Solids Struct. 45, 1845–1875.
Kraynik, A.M., Reinelt, D.A., van Swol, F., 2004. Structure of random foam. Phys. Rev. Lett. 93 (20). 208301/1-4.
Matzke, E.B., 1946. The three-dimensional shape of bubbles in foam – an analysis of the role of surface forces in three-dimensional shape determination. Amer. J. Botany 33, 58–80.
Montminy, M.D., Tannenbaum, A.R., Macosko, C.W., 2004. The 3D structure of real polymer foams. J. Colloid Interf. Sci. 280, 202–211.

Nieh, T.G., Higashi, K., Wadsworth, J., 2000. Effect of cell morphology on the compressive properties of open-cell aluminum foams. Mater. Sci. Eng. A 283, 105–110.
Papka, S.D., Kyriakides, S., 1994. In-plane compressive response and crushing of honeycomb. J. Mech. Phys. Solids 42, 1499–1532.
Papka, S.D., Kyriakides, S., 1998a. In-plane crushing of a polycarbonate honeycomb. Int. J. Solids Struct. 35, 239–267.
Papka, S.D., Kyriakides, S., 1998b. Experiments and full-scale numerical simulations of in-plane crushing of a honeycomb. Acta Mater. 46, 2765–2776.
Perrot, C., Panneton, R., Olny, X., 2007. Periodic unit cell reconstruction of porous media: application to open-cell aluminum foams. J. Appl. Phys. 101. 113538/1-11.
Weaire, D., Hutzler, S., 1999. The Physics of Foams. Oxford University Press, Oxford.
Zhou, J., Mercer, C., Soboyejo, W.O., 2002. An investigation of the microstructure and strength of open-cell 6101 aluminum foams. Metall. Mater. Trans. A 33, 1413–1427.
Zhou, J., Shrotriya, P., Soboyejo, W.O., 2004. Mechanisms and mechanics of compressive deformation in open-cell Al foams. Mech. Mater. 36, 781–797.
Zhou, J., Soboyejo, W.O., 2004. Compression-compression fatigue of open cell aluminum foams: macro-/micro- mechanisms and the effect of heat treatment. Mater. Sci. Eng. A 369, 23–35.
Zhou, J., Allameh, S., Soboyejo, W.O., 2005. Microscale testing of the strut in open cell aluminum foams. J. Mater. Sci. 40, 429–439.